Separation Science and Technology
Publication details, including instructions for authors and subscription information:
http://www.informaworld.com/smpp/title~content=t713708471

Adsorption of CO_2 on Hydrotalcite-like Compounds in a Fixed Bed

R. F. P. M. Moreira[a]; J. L. Soares[a]; G. L. Casarin[a]; A. E. Rodrigues[b]
[a] Departamento de Engenharia Química e Engenharia de Alimentos, Universidade Federal de Santa Catarina, Campus Universitário-Trindade, Florianópolis, SC, Brazil [b] Laboratory of Separation and Reaction Engineering-LSRE, Faculdade de Engenharia da Universidade do Porto-FEUP, Porto, CP, Portugal

To cite this Article Moreira, R. F. P. M. , Soares, J. L. , Casarin, G. L. and Rodrigues, A. E.(2006) 'Adsorption of CO_2 on Hydrotalcite-like Compounds in a Fixed Bed', Separation Science and Technology, 41: 2, 341 — 357
To link to this Article: DOI: 10.1080/01496390500496827
URL: http://dx.doi.org/10.1080/01496390500496827

Separation Science and Technology, 41: 341–357, 2006

ISSN 0149-6395 print/1520-5754 online
DOI: 10.1080/01496390500496827

Adsorption of CO_2 on Hydrotalcite-like Compounds in a Fixed Bed

R. F. P. M. Moreira, J. L. Soares, and G. L. Casarin
Departamento de Engenharia Química e Engenharia de Alimentos, Universidade Federal de Santa Catarina, Campus Universitário-Trindade, Florianópolis, SC, Brazil

A. E. Rodrigues
Laboratory of Separation and Reaction Engineering-LSRE, Faculdade de Engenharia da Universidade do Porto-FEUP, CP, Porto, Portugal

Abstract: The reduction of carbon dioxide emission from flue gases can be achieved using post-combustion technologies, such as adsorption employing efficient solid sorbents. In this work, the adsorption of CO_2 on hydrotalcite-like Al-Mg compounds partially carbonated was studied using dynamic and static methods. The breakthrough curves were obtained at different flow gas rates in the range 60 to 100 mL/min and total pressure 1.0 atm. Different mixtures of CO_2 diluted in helium were used (3–20% v/v) at temperatures in the range 29 to 350°C. The experimental equilibrium data were described according to a Langmuir-like equation. The capacity of adsorption presented a weak dependence on the temperature due to opposite effects of increasing of entropy and increasing of MgO (non-carbonated) content in the adsorbent at high temperatures. The linear driving force model was suitable to describe the breakthrough curves. The dispersion and mass transfer coefficients were calculated by theoretical correlations and the model described quite very well the adsorption of CO_2 on hydrotalcite-like compounds in a fixed bed in any temperature.

Keywords: Breakthrough curves, CO_2, hydrotalcite-like compounds, isotherms, greenhouse gases

Received 5 July 2005, Accepted 7 November 2005
Address correspondence to R. F. P. M. Moreira, Departamento de Engenharia Química e Engenharia de Alimentos, Universidade Federal de Santa Catarina, Campus Universitário-Trindade, CEP 88040-900, Florianópolis, SC, Brazil. Fax: (048) 331 9687; E-mail: regina@enq.ufsc.br

INTRODUCTION

The emission of carbon dioxide from burning fossil fuels has been identified as the major contributor to global warming and climate change. In the 1980s, carbon dioxide-containing flue gases contributed up to 25% of the global CO_2 emission and were responsible for 14% of the estimated global warming (19).

Separation and capture of CO_2 have been studied recently and the goal of CO_2 separation and capture is to isolate CO_2 from its many sources in a form suitable for transport and sequestration. There are three pathways for CO_2 separation: pre-combustion decarbonation, O_2/CO_2 recycle combustion, and post combustion separation (21). The steam reform of methane is a typical pre-combustion decarbonization process since the fuel is reacted with steam to produce mainly CO and H_2. The CO is processed in a catalytic reactor to give CO_2 and more H_2. The CO_2 is separated and the hydrogen can be used as fuel or in a hydrogen fuel cell (4, 5).

Several solid sorbents have been utilized to remove carbon dioxide in post combustion separation processes. Carbon molecular sieve-based material functionalized with amine groups, amine surface-bonded silica gel (13), acrylic ester resin-based solid amine sorbent (2), calcium oxides (23), magnesium silicates, and hydrotalcites (25) are shown to be suitable adsorbents to capture CO_2 in the gas phase. The ability to regenerate an adsorbent and the ease of this regeneration are also important considerations. The need for extreme conditions such as high temperatures or very low vacuum makes regeneration more complicated and costly.

It has been reported that hydrotalcite is a more suitable adsorbent of CO_2, especially at high temperatures. Hydrotalcites are anionic clays that present layers of positively-charged metallic oxide (or metallic hydroxide) with inter-layers of anions, such as carbonates. These materials have been studied by several authors (4, 5, 18, 22, 24, 25) for carbon dioxide adsorption, and their applicability in separation-enhanced reaction processes for methane steam-reforming has recently been reported, since these materials adsorb selectively the CO_2 produced by the reactions at high temperature (4, 5, 24). The amount of CO_2 removed by hydrotalcite depends on its pre-treatment (4) but there is no consensus about the importance of the chemisorption (7) and the effect of the previous contact with steam or CO_2 (4). Also the regeneration of these adsorbents is generally difficulty since a certain portion of CO_2 could be irreversibly chemisorbed on the material (7).

In this paper, we evaluated the CO_2 adsorption onto a hydrotalcite-like Al-Mg compound partially carbonated at the temperature range 29 to 350°C under different gas concentrations and total flowrate, and we also simulate the dynamic behavior in a fixed bed.

Breakthrough Curves

The mass balance in the column and the stoichiometric times, t_{st}, are given in Eqs. (1) and (2).

$$q^*(C_o) = \frac{QC_o t_{st}}{V(1-\varepsilon)} - \frac{\varepsilon C_o}{(1-\varepsilon)} \tag{1}$$

where

$$t_{st} = \int_0^\infty \left(1 - \frac{QC}{Q_o C_o}\right) dt \tag{2}$$

The rate of mass transfer of CO_2 to the solid is described according to the linear driving force model (6). The mass balance equation and boundary conditions are presented in Eqs. (3–6). The global mass balance applied to diluted gas feed in the column is given by Eq. (3) (15).

$$\frac{\partial C}{\partial \theta} + \frac{\rho_b}{\varepsilon}\frac{\partial \bar{q}}{\partial \theta} = \frac{1}{Pe}\frac{\partial^2 C}{\partial x^2} - \frac{\partial C}{\partial x} \tag{3}$$

The rate of mass transfer inside the particle is described by Eq. (4), and the mass transfer in the film around the particle is given by Eq. (5) (15).

$$\frac{\partial \bar{q}}{\partial \theta} = K_s \tau (q^* - \bar{q}) \tag{4}$$

$$\frac{\partial \bar{q}}{\partial \theta} = K_F a \tau (C - C_S) \tag{5}$$

The initial and boundary conditions are presented in Eq. (6) (15):

$$\begin{aligned} &\theta = 0; \quad \bar{q} = 0; \quad C = 0; \quad C_S = 0 \\ &x = 0; \quad -\frac{1}{Pe}\cdot\frac{\partial C}{\partial x} + C = C_{Feed} \\ &x = 1; \quad \frac{\partial C}{\partial x} = 0 \end{aligned} \tag{6}$$

The adsorption isotherms for CO_2 onto hydrotalcite is described according to a Langmuir-like equation Eq. (7).

$$q^* = \frac{q_m \,.\, b \,.\, C_s}{1 + b \,.\, C_s} \tag{7}$$

EXPERIMENTAL SECTION

Pellets of a hydrotalcite-like compound (MG50-Sasol) containing aluminum-magnesium hydroxide (length and diameter averages of 0.45 cm and 0.46 cm,

respectively) were used. The hydrotalcite-like MG-50 was characterized by BET, TGA and XRD techniques.

The equilibrium of CO_2 adsorption on MG-50 at temperatures in the range 29–350°C was studied in a fixed bed column. The sample was previously treated at 150°C for 4 hours in a helium atmosphere. Subsequently, CO_2 was passed during 24 hours through the fixed bed at oven temperature (29–350°C) followed by purge in helium at 150°C for 4 hours. This procedure was adopted to guarantee that chemical reactions (8) had occurred.

The breakthrough curves were obtained using CO_2 diluted in helium at different concentrations and total pressure 1.0 atm. The outlet gases at the end of the adsorption column were periodically analysed by gas chromatograph (CG 35—Instrumentos Científicos) using a thermal conductivity detector (TCD). The adsorption isotherm was determined by dynamic method at different concentrations of CO_2 in the gas phase at each temperature.

Characterization of the Adsorbent

Scanning electron microscopy/energy dispersive X-Ray (SEM/EDAX) was performed with a JEOL JSM 6301F. Elemental micro-probe and elemental distribution mapping techniques were used to analyze the composition of solids.

The characterization of the adsorbent was performed x-ray diffraction (XRD), thermal gravimetric analysis (TGA) and N_2 adsorption at 77 K. X-ray powder diffraction patterns were recorded on a Phillips instrument using CuKα Thermogravimetric analyses were carried out on a NETZSCH STA 409 simultaneous TG/DTA instrument.

The adsorption of N_2 at 77 K was performed using an Autosorb-1C adsorptometer (Quantachrome, USA). Before the analysis, the sample was thermally treated at 150°C under vacuum for 4 hours.

Breakthrough Curves of CO_2 Adsorption on Hydrotalcite-like MG50 in a Fixed Bed Column

The breakthrough curves were obtained at a temperature range of 29 to 350°C. The volume of the cylindrical column (diameter 2.14 cm, length 36.5 cm) allowed the accommodation of 1,045 pellets of adsorbent, and the bed porosity was 0.42.

After pre-treatment, the temperature of the column was adjusted to the desired value and a mixture of CO_2 diluted in helium was fed to a fixed bed column containing MG50. The total gas flow was in the range 60 to 100 mL/min with 1.0 of total pressure. Different mixtures of CO_2 diluted in helium were used.

The inlet and outlet tubes in the column were of external nominal diameter $1/16''$ to minimize dead volume. The flow was monitored by a mass flow control (MFC) and also checked by a film flowmeter, placed at the outlet of the column. The concentration and flow rate values were all measured and evaluated at temperature of the column.

Aliquots of the outlet gases at the end of the column were collected at regular times and injected into a gas chromatograph (CG35—CG Instrumentos Científicos, Brazil) equipped with a thermal conductivity detector (TCD) and a Porapak-Q column. Figure 1 gives a schematic presentation of the experimental apparatus.

Thermal Gravimetric Analysis—TGA

The TGA was performed to evaluate the thermal behavior of the adsorbent at different temperatures. Thermogravimetric analyses were carried out on a NETZSCH STA 409 simultaneous TG/DTA instrument. A heating rate of $10^{\circ}C/min$ was used in a nitrogen atmosphere. All data were obtained using platinum crucibles.

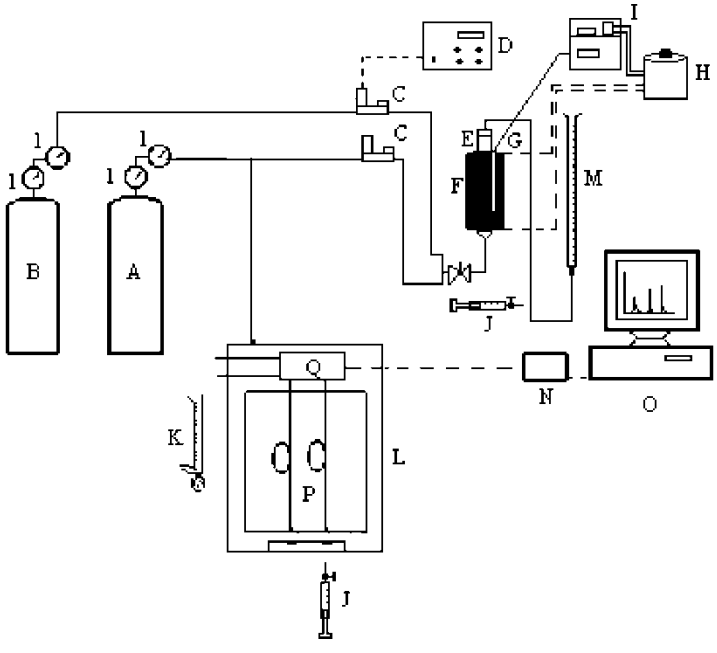

Figure 1. Schematic representation of the experimental system. (A) Helium; (B) CO_2; (C) Mass flow controller (MFC); (D) MFC control unit; (E) Adsorption column; (F) Oven; (G) Thermocouple; (H) Voltmeter (I) Temperature control unit; (J) Syringe sample; (K) Film flowmeter; (L) Gas chromatograph; (M) Film flowmeter; (N) Data acquisition system; (O) Computer; (P) Columns; (Q) TCD; (1) Bourdon manometers.

X-Ray Diffraction—XRD

X-ray powder diffraction patterns were recorded on a Phillips instrument using CuKα_1 radiation for five different treatments of the MG50: no treatment (virgin sample), after adsorption equilibrium of CO_2 at 150°C, after adsorption equilibrium of CO_2 at 250°C, after adsorption of CO_2 at 400°C, after adsorption of CO_2 and regeneration under helium at 400°C.

RESULTS AND DISCUSSION

Characterization of MG50

The main characteristics of the hydrotalcite-like MG50 are shown in Table 1. The solid is microporous and the BET surface area is typical for these materials (17).

Thermogravimetric Analysis

The thermogravimetric analysis results for the hydrotalcite-like submitted to different treatments are shown in Fig. 2. The fresh sample (Fig. 2a) presented only two peaks in the temperature ranges 80–100°C and 200–300°C due to the removal of residual water adsorbed on the surface and dehydration of the hydroxide group, respectively Eqs. (8) and (9) (3).

$$4\,MgCO_3 \cdot Mg(OH)_2 \cdot 4\,H_2O \longrightarrow 4\,MgCO_3 \cdot Mg(OH)_2 + 4\,H_2O \quad (T < 250^{\circ}C) \tag{8}$$

$$4\,MgCO_3 \cdot Mg(OH)_2 \longrightarrow 4\,MgCO_3 + MgO + H_2O \quad (250^{\circ}C < T < 350^{\circ}C) \tag{9}$$

Table 1. Characterization of hydrotalcite-like MG50

$MgO : Al_2O_3$ (%)	46.7 : 53.3
Pellet length (cm)	0.45
Pellet diameter (cm)	0.46
Pellet volume (cm^3)	0.048
Solid density (g/cm^3)[a]	3.07
Pellet density (g/cm^3)	1.13
Solid porosity	0.63
BET surface area (m^2/g)	154
Micropore volume (cm^3/g)[b]	0.0574
Micropore width (A)[c]	5.53

[a]Helium picnometry.
[b]N_2 adsoption at 77 K - DR method.
[c]N_2 adsoption at 77 K - HK method.

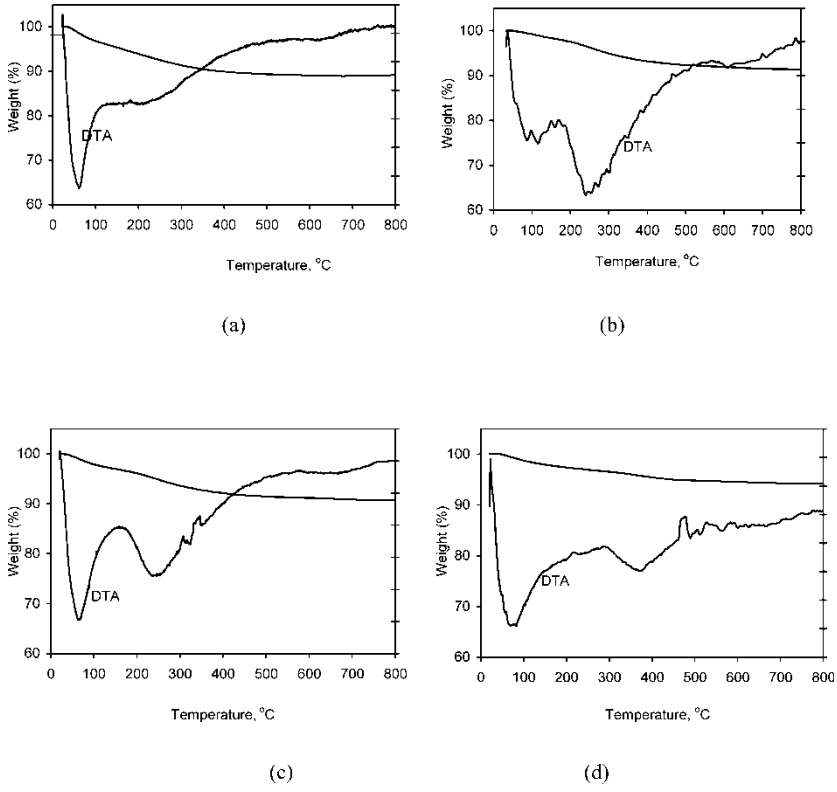

Figure 2. TGA and DTA curves for hydrotalcite-like MG50: (a) virgin; (b) saturated with CO_2 at 29°C; (c) regenerated by thermal treatment at 150°C under helium atmosphere; (d) regenerated by thermal treatment at 250°C under helium atmosphere.

Figure 2b shows the weight loss of the hydrotalcite-like MG50 that was saturated with CO_2 at 29°C and subsequently submitted to TGA analysis. A broad peak ascribed to the dehydroxilation reaction (Eq. 10) can be observed in the temperature range 200–300°C that was also present in the sample regenerated at 150°C (Figure 2c), but it did not appear in the sample regenerated at 250°C (Figure 2d).

The weight loss up to 350°C is somewhat controversial because some authors ascribed it to water elimination (3) or removal of carbonate ions Eq. 10) (1). Over this temperature range, hydrotalcite-like materials undergo dehydroxylation (Eq. 9) and decarbonation (Eq. 10) and release carbon dioxide and water. The weight loss observed in Fig. 2b–d could correspond to the removal of carbonate ions from the interlayer and hydroxide ions from hydrotalcite-like. It can be clearly observed in Fig. 2d a weight loss at temperatures above 370°C, due to the carbonate decomposition (Eq. 10), that could be covered in Figures 2b and 2c by the weight loss

owing to the dehydration reaction (Eq. 9) (3). In fact, the virgin sample does not present a significant weight loss up to 350°C, indicating that no $MgCO_3$ was present in the virgin sample.

$$4\,MgCO_3 \rightarrow 4\,MgO + 4CO_2 \quad (T < 350^{\circ}C) \tag{10}$$

X-Ray Diffraction—XRD

According to the manufacturer, the hydrotalcite-like adsorbent used in this work was previously calcinated at 500°C. The XRD spectrum of the virgin sample (Fig. 3E) shows a behavior that is typical for hydrotalcite materials calcinated at high temperatures (>450°C). Heating destroys the layered structure typical of hydrotalcites and yields a periclase MgO phase in addition to amorphous aluminum (1, 12, 20) and the results showed in Fig. 3E shows that periclase MgO is the sole crystalline phase in the adsorbent.

Valente *et al*. (20) have reported that these kind of mixed oxides can be reversibly rehydrated to the layered structure after exposure to water vapor. However, the adsorption of CO_2 and regeneration of the adsorbent was performed in absence of water vapor and then no crystalline modification was expected for the samples submitted to different treatments, as shown in Fig. 3A-D.

Equilibrium of CO_2 Adsorption MG50

According to the experimental protocol used as pre-treatment of the sample, it was expected a partial carbonation reaction in the pre-treatment at 29 and 60°C and near to equilibrium carbonation for pre-treatment at 150, 250, and 350°C. The carbonation reaction between MgO and gaseous CO_2 proceeds very slowly at room temperature and increases with temperature. However, if the temperature is raised too much the chemical equilibrium shifts so that free CO_2 is favored over the bound form (11).

Data on the chemical rate of the carbonation of magnesium-based minerals is scarce. In order to evaluate the fraction of MgO that was converted to $MgCO_3$ (Eq. 10) in the pre-treatment, it was considered the kinetic model (Eq. 11) proposed by (9).

$$-\frac{d(MgO)}{dt} = k_1(MgO)(P_{CO_2}) - k_{-1}(MgCO_3) \tag{11}$$

where (MgO) and ($MgCO_3$) represent the mass of MgO and $MgCO_3$, respectively and k_1 and k_{-1} are the kinetics constants for forward and reverse reactions (Eq. 10). The conversions of MgO to $MgCO_3$ after pre-treatment at different temperature were calculated and resulted in 2.4% and 13.4% at 29 and 60°C, respectively, and the equilibrium conversion value should be

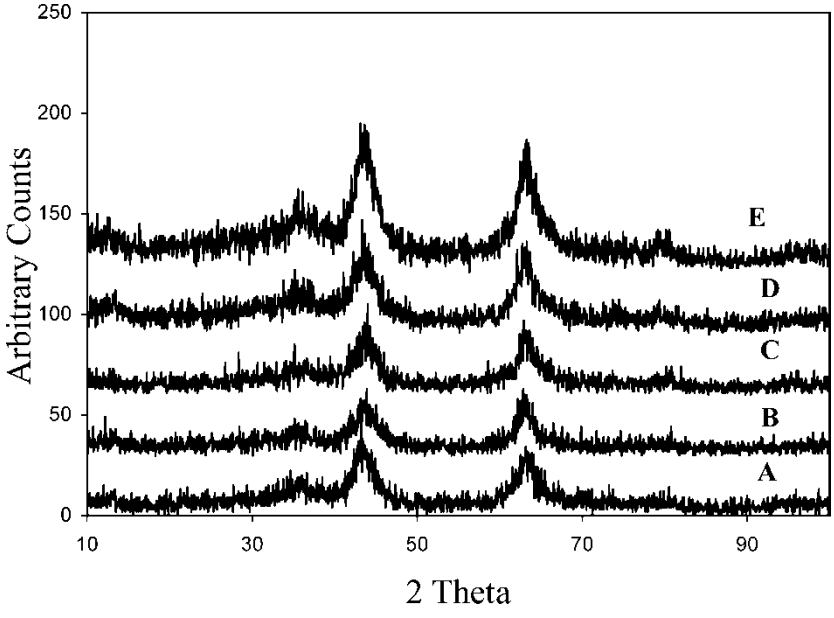

Figure 3. XRD patterns for hydrotalcite-like MG50: (A) after adsorption of CO_2 at 150°C; (B) after adsorption of CO_2 at 250°C; (C) after adsorption of CO_2 at 400°C; (D) After adsorption of CO_2 and regeneration under helium at 400°C; (E) Virgin sample.

achieved for pre-treatment at 150, 250 and 350°C (99.4%, 51.8% and 2.8%, respectively).

The removal equilibrium isotherms of CO_2 on MG50 at different temperatures are shown in Fig. 4. The CO_2 removal represents only the contribution of adsorption, because at low temperatures the carbonation reaction is negligible and at high temperature the carbonation reaction had achieved the thermodynamical equilibrium.

Several cycles of adsorption of CO_2 on hydrotalcite-like MG50 and re-activation under helium at 150°C have shown that the CO_2 adsorption is reversible (16) if the sample is previously contacted with carbon dioxide, and the capacity of adsorption is restorable after treatment at 150°C under helium.

The experimental results of the CO_2 adsorption at the equilibrium at different temperatures are summarized in Table 2.

The equilibrium data were fitted to a Langmuir-like equation and the equilibrium parameters are shown in Table 3. In all cases, the maximum error between experimental and theoretical error was 5%.

The capacity of adsorption of CO_2 on MG50 at 29°C is lower than the capacity using activated carbon (17). However, hydrotalcite-like MG50 presents high adsorption capacity at high temperatures, while activated

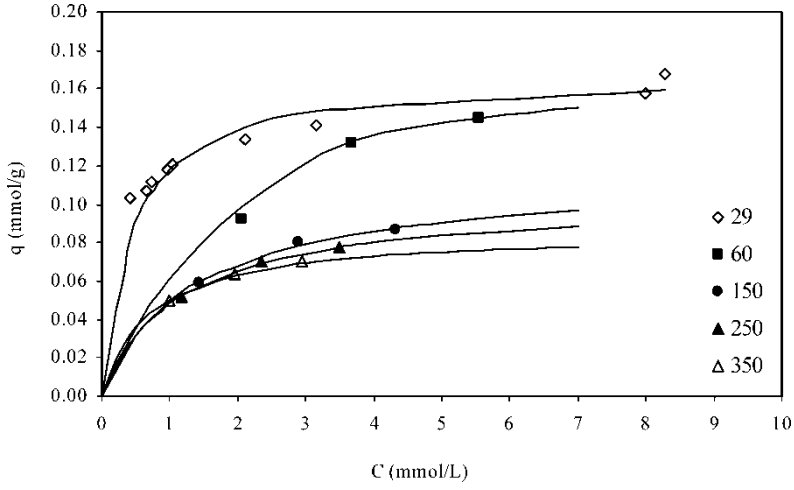

Figure 4. Adsorption of CO_2 on hydrotalcite-like MG50 at 60, 150, 250 and 350°C.

carbons do not have chemical stability at high temperature (25). Thus hydrotalcite is a more suitable adsorbent for the capture of CO_2 over a wide range of temperature.

In Table 3 it may be observed that the maximum amount of CO_2 adsorbed on MG 50 decreases with the increase of the temperature.

Considering the kinetics and equilibrium of carbonation reaction, the amount of available adsorbent (non-carbonated) corresponds to a 98%, 94%, 50%, 74%, and 99% of the total adsorbent at 29, 60, 150, 250, and

Table 2. Stoichiometric times and adsorption capacity for different concentrations of CO_2 and temperatures

T(°C)	$[CO_2]$ mol/L	t_{st} (min)	q (mmol/g)
60	1.831	24.7	0.092
	3.662	17.8	0.132
	5.493	14.0	0.155
150	1.441	15.9	0.059
	2.882	11.1	0.080
	4.323	7.8	0.087
250	1.166	14.1	0.052
	2.331	9.7	0.070
	3.496	6.9	0.077
350	0.979	13.5	0.050
	1.957	8.7	0.063
	2.936	6.1	0.069

Table 3. Parameters of the Langmuir-like equation at different temperatures

T (°C)	b (L/mmol)	q_m (mmol/g)
29	2.358 ± 0.012	0.168 ± 0.005
60	0.349 ± 0.003	0.236 ± 0.001
150	0.746 ± 0.078	0.115 ± 0.004
250	0.905 ± 0.061	0.102 ± 0.002
350	1.451 ± 0.001	0.085 ± 0.001

350°C, respectively. At temperature higher than 150°C, the equilibrium carbonation conversion decreases and high fraction of adsorbent is available for adsorption. Then the experimental results can be analyzed by considering entropic effects (which explain a decreasing of adsorption capacity as the temperature increases) and availability of adsorbent (which increases the adsorption capacity as the temperature increases). As a result, a weak dependence on the temperature can be observed in the amount CO_2 adsorbed at high temperature.

The complete capacity of CO_2 removal by reaction and adsorption could only be restored only by thermal treatment above 370°C, as shown in Fig. 2d.

Breakthrough Curves of Adsorption

The dynamics of the CO_2 adsorption in a fixed bed was described using the linear driven force model (LDF). The necessary parameters for the simulation of the adsorption breakthrough were evaluated by means of correlations from the literature.

The simulated breakthrough curves of adsorption were generated through the solution of Eqs. 3–8. Peclet's number of was evaluated according to Eq. (12) (15).

$$D_{ax} = \gamma_1 D_m + \gamma_2 d_{eq} v \tag{12}$$

where:

$$\gamma_1 = 0.45 + 0.55\varepsilon = 0.68$$
$$\gamma_2 = 0.5$$
$$d_{eq} = 0.52\text{cm}$$

The molecular diffusivity (D_m) was calculated by Chapman-Enskog correlation (14). The film mass transfer coefficient (K_F) around the particles was obtained by Eq. (13) (14, 15):

$$Sh = 2 + 1.1Sc^{1/3}Re^{0.6} \tag{13}$$

The constant of the linear driving force model (K_s) was fitted to minimize the average residual errors. Eqs. 3–8 were solved using the PDECOL package (10) in the FORTRAN language, which is based on the method of orthogonal collocation of finite elements for partial differential equations in double precision. Normally, 50 to 100 elements are used in the calculations, with two interior collocation points, 10^{-9} tolerance and 60 seconds that are needed for the numeric simulation of the breakthrough curves.

The breakthrough curves for the adsorption of CO_2 on MG50 at 29°C are shown in Fig. 5. It can be observed that the breakthrough is sharp, indicating a compressive front, and the breakthrough curves are symmetrical. Different CO_2 concentrations at the column inlet and gas flowrates resulted in the curves shown in Fig. 5.

The breakthrough curves in Fig. 5 were simulated using the parameters shown in Table 4. At 29°C, the K_S value that minimizes the average

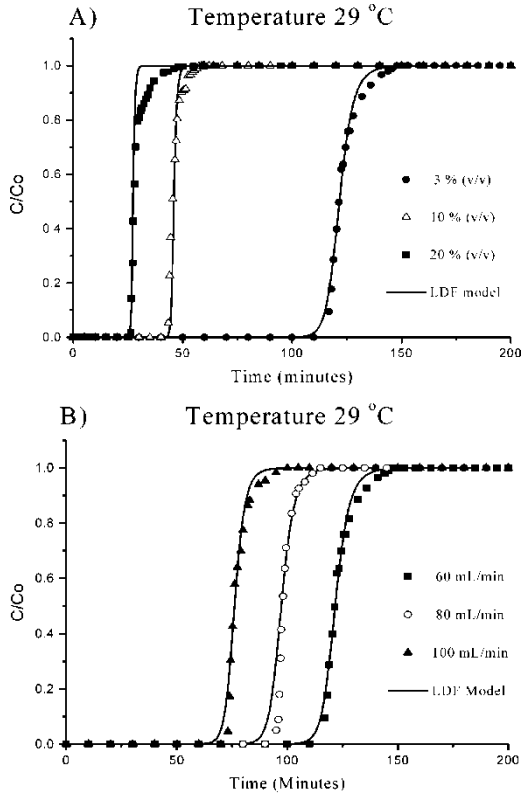

Figure 5. Breakthrough curves for the adsorption of CO_2 on hydrotalcite-like MG50: (a) different initial CO_2 concentration (total flowrate 60 mL/min and total pressure 1.0 atm); (b) different total flowrate (CO_2 concentration 3% v/v and total pressure 1.0 atm).

Table 4. Parameters used for the simulation of breakthrough curves

% CO_2 (v/v)	Gas flowrate, (mL/min)	Re	Pe	Sc	Sh	K_s, s^{-1}	K_F, (cm/s)
3	60	0.16	42.1	1.50	2.43	3.31×10^{-3}	2.75
	80	0.22	50.9	1.50	2.51	3.31×10^{-3}	2.86
	100	0.27	58.1	1.50	2.57	3.31×10^{-3}	2.93
10	60	0.26	42.1	0.94	2.48	3.31×10^{-3}	2.82
20	60	0.40	42.1	0.60	2.53	3.31×10^{-3}	2.88

residual errors is $3.31 \times 10^{-3}\,s^{-1}$ for all experiments under different flow rates and inlet CO_2 concentration (Table 4). Mass transfer resistance inside the solid particle could be expected as controlling mechanism at low temperature as shown in Fig. 5. The capacity of adsorption of CO_2 on MG is high at 29°C, and this result shows the flexibility of this material to capture CO_2 in the control of the greenhouse effect.

At high temperatures, simulations with the parameters from Table 5 agree with the experimental results (Fig. 6), indicating that the LDF model is suitable for the description of the adsorption of CO_2 on MG50 in a fixed bed.

The low Reynolds number corresponds to a laminar regime. The Peclet number ($Pe = v \cdot L/D_{ax}$) is almost independent on the temperature since the axial dispersion and gas velocity increase with temperature, and the film mass transfer also increases as the temperature increases.

CONCLUSIONS

Hydrotalcite-like MG50 presents good capacity of adsorption for the CO_2 at any temperature of operation The CO_2 removal is due to the carbonation reaction and adsorption. The CO_2 retained by reaction can only be released

Table 5. Parameters used to simulate the breakthrough curves for CO_2 adsorption on hydrotalcite-like MG50, obtained from literature correlations

T (°C)	60	150	250	350
$D_m(cm^2/s)$	0.707	1.043	1.483	1.992
Pe	13.87	12.38	11.10	10.04
Re	0.24	0.20	0.17	0.15
Sc	1.00	1.00	1.02	1.05
Sh	2.45	2.41	2.38	2.35
K_F (cm/s)	3.331	4.813	6.788	9.003
$K_S \times 10^2$ (s^{-1})	3.467	3.917	4.350	4.750

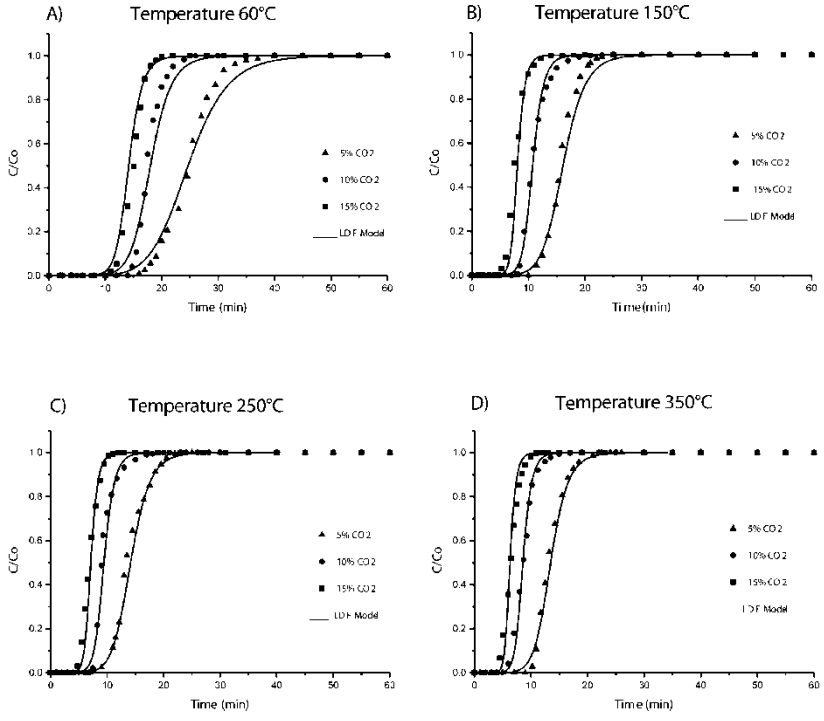

Figure 6. Breakthrough curves for CO_2 adsorption on hydrotalcite-like MG50 at different temperatures and 1.0 atm.

by thermal treatment at temperatures above 370°C. XRD studies showed that periclase MgO is the only crystalline phase in the adsorbent.

The equilibrium of adsorption showed a weak dependence with the temperature using hydrotalcite-like compound partially carbonated, since entropic effects and availability of adsorbent are opposite factors at temperatures higher than 150°C.

The CO_2 adsorption in a fixed bed shows that the axial dispersion and mass transfer increase as the temperature increases. The linear driving force model has been successfully fitted in order to describe the dynamics of CO_2 adsorption on hydrotalcite in a fixed bed.

Greek Letters

ε	Total bed porosity
λ	Constant
μ	Viscosity, kg/ms
θ	Dimensionless time, $[t/\tau]$

ρ_b	Bed density, kg/L
τ	Spatial time [L/v], min

NOMENCLATURE

a	External surface area for unit of volume of the pellet, cm^{-1}
b	Langmuir-like constant equilibrium, L/mmol
C	Molar concentration in the bulk phase, mol/L
C_o	Initial molar concentration, mol/L
C_S	Molar concentration on surface of the pellet, mol/L
d_{eq}	Equivalent sphere diameter for the cylindrical pellet, cm
D_{ax}	Axial mass dispersion coefficient, cm^2/s
D_m	Molecular diffusivity, cm^2/s
k	Equilibrium constant of Freundlich isotherm, mmol/g
K_F	Film's mass transfer coefficient, cm/s
K_S	Internal mass transfer coefficient, s^{-1}
L	Bed length, cm
n	Parameter of Freundlich isotherm
Pe	Peclet number, [v . L/Dax]
q	Adsorbed concentration, $mmol/g_{Pellet}$
$\bar{q}$	Adsorbed phase average concentration, $mmol/g_{Pellet}$
q^*	Adsorbed concentration at equilibrium, $mmol/g_{Pellet}$
q_m	Maximum adsorbed concentration, $mmol/g_{Pellet}$
Q_o	Inlet flow rate, mL/min
Q	Flow rate, mL/min
r_p	Pellet radius, cm
Re	Reynolds number, $[\rho . v . d_{eq}/\mu]$
Sc	Schmidt number, $[\mu/\rho.D_m]$
Sh	Sherwood number, $[K_F . d_{eq}/D_m]$
t	Time, min
t_{St}	Stoichiometric time, min
u	Superficial velocity, cm/s
v	Interstitial velocity, $[u/\varepsilon]$, cm/s
V	Bed volume, cm^3
x	Dimensionless axial coordinate in the bed [z/L]
z	Axial coordinate in the bed, m

REFERENCES

1. Aramendia, M.A., Avilés, Y., Benítez, J.A., et al (1999) Comparative study of Mg/Al and Mg/Ga layered double hydroxides. *Microporous and Mesoporous Materials*, 29: 319–328.
2. Birbara, P.J., Philip, J., Filburn, T.P., Nalette, T.A. (2002) Regenerable solid amine sorbent. US Patent 5,876,488.

3. Botha, A. and Strydom, C.A. (2001) Preparation of a magnesium hydroxy carbonate from magnesium hydroxide. *Hydrometallurgy*, 62: 175–183.
4. Ding, Y. and Alpay, E. (2000a) Equilibria and kinetics of CO_2 adsorption on hydrotalcite adsorbent. *Chemical Engineering Science*, 55: 3461–3474.
5. Ding, Y. and Alpay, E. (2000b) Adsorption-enhanced steam reforming. *Chemical Engineering Science*, 55: 3929–3940.
6. Glueckauf, E. (1955) The theory of chromatography. Part 10. Formulae for diffusion into spheres. Theory of chromatography. *Transactions of the Faraday Society*, 51: 1540–1551.
7. Hufton, J.R., Mayorga, S., and Sircar, S. (1999) Sorption-enhanced reaction process for hydrogen production. *AIChE Journal*, 45: 248–256.
8. Khan, N., Dollimore, D., Alexander, K., and Wilburn, F.W. (2001) The origin of the exothermic peak in the thermal decomposition of basic magnesium carbonate. *Thermochimica Acta*, 367–368, 321–333.
9. Kohlmann, J., Zevenhoven, R., and Mukherjee, A.B. (2002) Carbon dioxide emission conrol by mineral carbonation: the option for Finland, Proceedings of the 6th European Conference of Industrial Furnaces and Boilers, 1–8.
10. Madsen, N.K. and Sincovec, R.F. (1979) PDECOL: General collocation software for partial differential equations. *ACM Transactions on Mathematical Software*, 5: 326–351.
11. Lackner, H.S., Wendt, C.H., Butt, D.P., Joyce, E.L., and Sharp, D.H. (1995) Carbon dioxide disposal in carbonate minerals. *Energy*, 20: 1153–1170.
12. Lanas, J. and Avarez, J.I. (2004) Dolomitic Lime: Thermal decomposition of nesquehonite. *Thermochimica Acta*, 421: 123–132.
13. Leal, O., Bolívar, C., Ovalles, C., et al (1955) Reversible adsorption of carbon dioxide on amine surface-bonded silica gel. *Inorganica Chimica Acta*, 240: 183–189.
14. Ratto, M., Lodi, G., and Costa, P. (1996) Sensitivity analysis of a fixed-bed gas-solid TSA: The problem of design with uncertain models. *Separation Technology*, 6: 235–245.
15. Ruthven, D.M. (1984) *Principles of Adsorption and Adsorption Processes*. John Wiley & Sons: New York.
16. Soares, J.L., Grande, C.A., Yong, Z., et al (2002) Adsorption of carbon dioxide at high temperatures onto hydrotalcite-like compounds (HTlcs). *Fundamentals of Adsorption*, 7: 78–83.
17. Soares, J.L. (2003) Desenvolvimento de novos adsorventes e processos híbridos em reforma catalítica sob vapor de água, PhD Thesis. Federal University of Santa Catarina: Florianópolis, Brazil.
18. Soares, J.L., Moreira, R.F.P.M., José, H.J., et al (2004) Hydrotalcite materials for carbon dioxide adsorption at high temperatures: characterization and diffusivity measurements. *Separation Science and Technology*, 39: 1989–2010.
19. Soong, Y., Schoffstall, M.R., Gray, M.L., et al (2001) Dry beneficiation of high loss-on-ignition fly ash. *Separation and Purification Technology*, 26 (2–3): 177–184.
20. Valente, J.S., Figueras, F., Gravelle, M., et al (2000) Basic properties of the mixed oxides obtained by thermal decomposition of hydrotalcites containing metallic compositions. *Journal of Catalysis*, 189: 370–381.
21. Wong, S. and Bioletti, R. (2004) Carbon dioxide separation technologies. *Interamerican Association of Sanitary and Environmental Engineering*, : 1–14.

22. Xiu, G.H., Soares, J.L., Li, P., and Rodrigues, A.E. (2002) Pressure swing adsorptive reactors: Simulation of five-step one-bed sorption-enhanced reaction processes. *AIChE Journal*, 48: 2817–2832.
23. Yi, K.B. and Harrison, D. (2005) Low-pressure sorption-enhanced hydrogen production. *Industrial and Engineering Chem. Res*, 44: 1665–1669.
24. Yong, Z., Mata, V., and Rodrigues, A.E. (2001) Adsorption of carbon dioxide onto hydrotalcite-like compounds (HTlcs) at high temperatures. *Industrial and Engineering Chemical Research*, 40: 204–209.
25. Yong, Z., Mata, V., and Rodrigues, A.E. (2002) Adsorption of carbon dioxide at high temperature—A review. *Separation and Purification Technology*, 26: 195–205.